AIChE

Increased Gas Solubility in Nanoliquids: Improved Performance in Interfacial Catalytic Membrane Contactors

Marc Pera-Titus, Sylvain Miachon, and Jean-Alain Dalmon
Institut de Recherches sur la Catalyse et l'Environnement de Lyon (IRCELYON),
UMR 5256 CNRS—University of Lyon 2, av. A. Einstein, 69626 Villeurbanne cedex, France

DOI 10.1002/aic.11656
Published online December 17, 2008 in Wiley InterScience (www.interscience.wiley.com).

The kinetics of gas-liquid catalytic reactions can be strongly promoted when these are performed in interfacial catalytic membrane reactors instead of other three-phase reactors such as slurry stirrers or trickle beds. The well-defined gas-liquid-catalyst contact in this system avoiding diffusional limitations is usually argued as the main reason for such enhancement. In this work, using nitrobenzene hydrogenation as a model reaction, we propose that this increased catalytic performance might also be attributed, at least partially, to increased gas solubilities in mesoconfined solvents (or simply "nanoliquids") in interfacial contactors overcoming the values predicted by Henry's Law. To support this hypothesis, we provide experimental evidence of a dramatic increase of H_2 solubility in confined ethanol using mesoporous γ-Al_2O_3 as confining solid. Gas-liquid solubilities can be enhanced up to five times over the corresponding bulk values for nanoliquid sizes lower than 15 nm as long as the gas-liquid interface is confined in a mesoporous array. In such a situation, the volume of the gas-liquid interface is no longer negligible compared to the total volume of the confined liquid, and the high surface excess concentrations of the gas adsorbed on the liquid surface make solubility grow up dramatically. According to these measurements, we discuss how nanoliquids might form in catalytic membrane contactors, which gas-liquid configuration in the reactor appears to be more appropriate, and how the structure of the mesoporous catalytic layer contributes to their increased gas solubilization performance. © 2008 American Institute of Chemical Engineers *AIChE J,* 55: 434–441, 2009
Keywords: catalytic membrane contactor, nanoliquid, solubility, hydrogenation, nitrobenzene

Introduction

Catalytic membrane reactors (CMRs) have attracted attention because of their advantages related to the synergy of the catalyst and membrane when implemented in the same device. Within this family, interfacial contactors CMRs (icCMRs) are characterized by a triple contact between two different reactant fluid phases (usually gas-liquid contact) and the catalyst.[1–3] This helps circumventing diffusional resistances to mass transfer, leading to higher catalytic activities than other three-phase reactors (e.g., slurry stirrers and trickle-beds).[3,4] Moreover, the catalyst being part of the reactor, its recovery does not need any separation from the liquid medium.

Interfacial catalytic membranes usually consist of multilayered tubular ceramic tubes (usually made of alumina, titania, zirconia or titania coated with titania depending on the application[4–6]) with decreasing pore size from the outer to the

Correspondence concerning this article should be addressed to M. Pera-Titus at marc.pera-titus@ircelyon.univ-lyon1.fr.

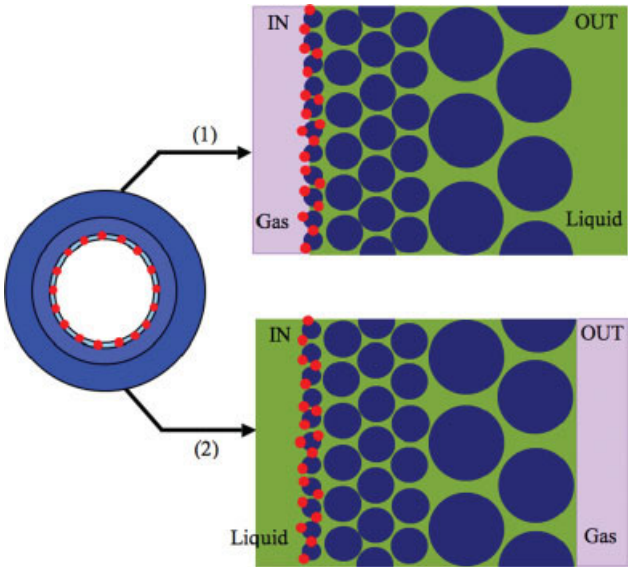

Figure 1. Gas-liquid configurations in multilayered interfacial CMRs: (1) Gas in, liquid out; (2) gas out, liquid in.

The small and larger cycles refer, respectively, to the catalyst and alumina grains of the membrane structure. [Color figure can be viewed in the online issue, which is available at www.interscience.wiley.com.]

inner layer, this latter lying in the mesoporous range and containing most of the catalyst, for instance, Pt (see Figure 1). The catalyst is usually dispersed in the mesoporous layer by ionic impregnation or evaporation-crystallization with a convenient precursor (e.g., hexachloroplatinic acid in the case of Pt deposition) and activated by reduction under H_2 flow at 673 K.[7,8] Using this procedures, Pt nanoparticles up to 1.5 nm in size can be synthesized with loadings in the contactor up to 1.5 wt % for mean pore sizes lying in the range 5–20 nm.[4]

The position of the gas-liquid interface within the membrane thickness plays a relevant role in the performance of icCMRs, as has been reported in several studies.[9–11] Higher reaction rates are achieved by locating the gas-liquid interface as close as possible to the catalytic zone. In this way, two gas-liquid configurations can be defined, as shown in Figure 1: (1) liquid flowing outside and gas flowing inside (liquid out, gas in), and (2) gas flowing outside and liquid flowing inside (gas out, liquid in).

In this context, the first experiments carried out by our group during the 90s using nitrobenzene hydrogenation as a model reaction[4] revealed a zero-order kinetics for hydrogen in an interfacial contactor CMR operated using configuration 1 for mean pore sizes of the mesoporous layer lower than 25 nm. Above this value, the kinetics turns into first order for hydrogen. An apparent first order for hydrogen is also found when operating with icCMRs in configuration 2 as well as for slurry-type reactors in absence of diffusion limitations. Table 1 summarizes the most relevant information related to the kinetics of this reaction for the different configurations of interfacial-type catalytic contactors and slurry-type reactors. These observations suggest that, in configuration 1, gas access is not a limiting factor, the H_2 coverage of the catalyst active surface being much higher in this case. This translates into rate enhancement factors up to 5 when compared to configuration 2 and similar reaction rates to those obtained in a model slurry-type reactor. This improved efficiency has also been observed in other recent applications of gas-liquid catalytic membrane contactors, for instance, in the catalytic wet air oxidation of formic acid, conceived and developed in the framework of the WaterCatox European project.[14–16] In this article, we will concentrate our attention on nitrobenzene hydrogenation.

It is known that, at the scale of a few nanometers, the physicochemical properties of condensed matter differ from their corresponding macroscopic values.[17,18] In this way, it has been suggested that the enhanced catalytic activity of membrane contactors might be at least partially attributed to increased gas solubilities in the solvent confined in the mesopores of a membrane.[4] This idea is sustained by a recent experimental study performed by our group,[18] where the solubility of H_2 and light hydrocarbons in different solvents confined in the cavities of mesoporous γ-alumina and silica has been measured using a methodology based on proton nuclear magnetic resonance (^{1}H-NMR). These results revealed that, in all cases, one or two signals ascribed to the dissolved gas in the mesoconfined solvent could be identified after peak deconvolution. Liquid confinement appears to promote gas solubility by three to five times over the corresponding macroscopic values. Moreover, gas solubility increases dramatically when tuning the nanoliquid size to values lower than 15 nm. Moreover, gas solubility appears to be only promoted when the gas-liquid interface is localized in the solid mesopores, suggesting an important role of surface excess concentrations at the gas-liquid interface in the measured solubilities.

To provide more insight into this phenomenon and its implications in the performance of interfacial contactors CMRs, herein, we report the measurement of H_2 solubility in mesoconfined ethanol (solvent used in[4] for nitrobenzene hydrogenation) by microvolumetry. Also, the confining solid used in this study is the same as the membrane material, γ-alumina. Our major goal is to describe how nanoliquids are formed and behave in interfacial contactors CMRs, and to discuss the influence of the gas-liquid configuration and the mean size of the mesoporous layer in its catalytic performance.

Experimental

Materials

Ethanol (purity > 99.9%), supplied by Sigma-Aldrich (Germany), was used as solvent. Hydrogen gas (purity >

Table 1. Summary of Kinetic Data for the Reaction of Nitrobenzene (NB) Hydrogenation Catalyzed by Pt/γ-Al_2O_3

Reactor	Apparent H_2 Order	Apparent NB Order	Catalytic Activity ($\times 10^{10}$ mol s^{-1} cm^{-2} Pt)	Refs.
(1)	0	0.3–0.6	9.5	4
(2)	1	0	2.0	4,12
Slurry	1	0	10	13

Experimental conditions: NB, 0.62 mmol L^{-1}; H_2 pressure, 101 kPa; temperature, 313 K; ΔP, 50 mbar. The reactor type refers to the configurations described in Figure 1.

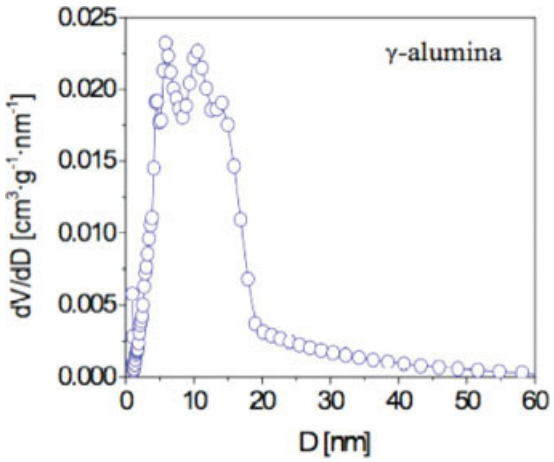

Figure 2. Pore size distribution of γ-alumina, as obtained from nitrogen adsorption at 77 K.

[Color figure can be viewed in the online issue, which is available at www.interscience.wiley.com.]

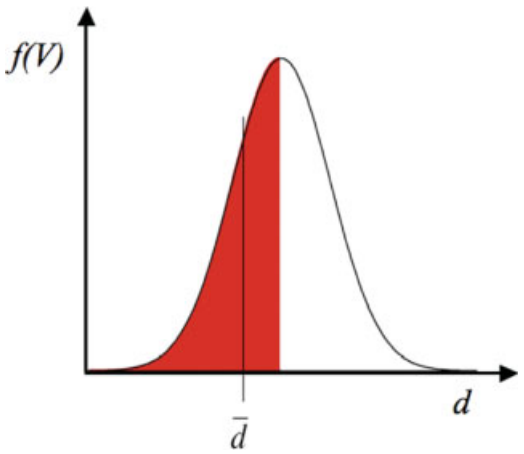

Figure 3. Mean pore size, $\bar{d}$, filled by the liquid according to the liquid loading of the confining solid volumetric pore-size distribution.

[Color figure can be viewed in the online issue, which is available at www.interscience.wiley.com.]

99.99%) was obtained from Air Liquide (France). The confining solid was γ-alumina GFS-400, with skeletal density of 3.5 g cm^{-3}, measured by microvolumetry using He, 235 m^2 g^{-1} specific surface, 0.62 cm^{-3} g^{-1} Broekhoff-de-Boer (BDB) pore volume and 10.9 nm mean pore size, as measured on our premises by N_2 adsorption at 77 K. The corresponding pore size distribution obtained by the BDB method is shown in Figure 2.

The mean pore size of γ-alumina filled up by the liquid (also referred later as *nanoliquid size*) was computed from the BDB pore size distribution of the solid by considering the liquid loading of the solid. In these calculations, on the basis of the form of the adsorption/desorption isotherm of ethanol on mesoporous γ-alumina (Type V), it was implicitly assumed that pore filling takes place from smaller to larger pores according to the Kelvin equation. The nanoliquid mean size, $\bar{d}$, for a given liquid loading, f, was computed and tuned from the pore volume distribution (BDB, from N_2 desorption at 77 K) by Eq. 1, where the pores have been assumed to be slit-like (see Refs. 19,20 for further details):

$$\bar{d} = \left[\frac{1}{V(f)} \int_0^{V(f)} (d - 2t)^3 \delta V \right]^{1/3} \quad (1)$$

where $2t$ is the statistical thickness of the pore wall. The effect of pore filling on average nanoliquid size can be visualized in Figure 3. The application of bulk density values to mesoconfined ethanol is well supported by Morishige and Shikimi[21] and Tzevelekos et al.[22]

Set-up

Gas solubility was measured by microvolumetry. The set-up used for this purpose consisted of two units (see Figure 4). Unit 1 included a stainless steel cell of perfectly known volume, a calibrated reference volume, a differential pressure gauge (Rosemont 3051, Emerson Process Management, USA, accuracy <0.06% full scale, 0–630 mbar), and two total pressure gauges (Keller AG, Jestetten, Germany, 0–20 bar and 0–400 mbar, respectively) to carry out the microvolumetry measurements. Compared to the methodology used in a previous work relying on ^{1}H-NMR analysis,[19] microvolumetry is not limited to proton-free solvents, and the measurements are faster and easier to perform.

Unit 2 includes a primary vacuum line equipped with a membrane pump (MVP 035-2, Pfeiffer Vacuum Technology, Germany) to evaporated fixed amounts of solvent in the cell, and a secondary vacuum line provided with a turbomolecular pump (TMH 071, Pfeiffer Vacuum Technology, Germany, maximum pressure $<10^{-7}$ mbar) for previous outgassing of the target solid in the cell. A cold trap cooled with liquid nitrogen was placed between both units for vapor condensation. Further details on this experimental system can be found elsewhere.[20]

Measurement of gas solubilities

Some preliminary solubility experiments of H_2 in bulk ethanol previously degassed in an ultrasonic bath and *in situ* revealed that the concentration of dissolved H_2 increases linearly with pressure according to Henry's Law, the solubilities matching the literature values (see Table 2). This validates the measurement technique.

In the case of confining the target solvent in the porous solid, prior to any measurement, the solid placed in the cell

Table 2. Values of H_2 Solubility in Ethanol at 101 kPa in Different Liquid-Solid Environments Using γ-Al_2O_3 as Confining Solid

System at Equilibrium with Gas Phase	ℓ_{H2} [%]
(1) Bulk solvent	5 ± 2 (8.7)*
(2) Bulk solvent with porous solid	10 ± 3
(3) Solvent confined in mesopores (average diameter 4 nm)	45 ± 7

The gas pressure was kept at 100–120 kPa in all experiments.
*Value obtained from Ref. 23.

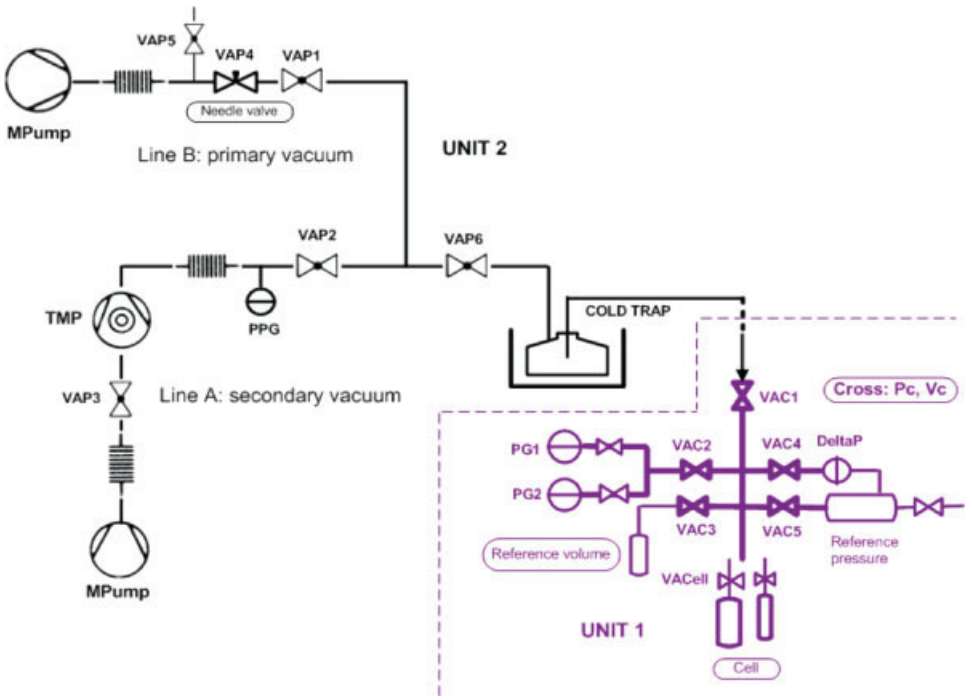

Figure 4. Scheme of the microvolumetry set-up used to measure gas solubility values.

Nomenclature: PG, absolute pressure gauge (piezo); DeltaP, differential pressure gauge; PPG, pumping pressure gauge (Pirani + cold cathode); VACell, isolation valve cells; TMP, turbomolecular pump; MPump, membrane pump; VAC, Valve cross zone (unit 1); VAP, valve pumping zone. [Color figure can be viewed in the online issue, which is available at www.interscience.wiley.com.]

was first outgassed at 423 K for at least 3 h under secondary vacuum ($<10^{-4}$ mbar). Subsequently, the volume of the solid was measured from He expansion, and blank H_2 adsorption tests were performed on dry γ-alumina by microvolumetry (the H_2 loading was as low as ~ 2 μmol g^{-1} at 101 kPa). The solid was then soaked with a large volume of solvent previously degassed in an ultrasonic bath for 15–30 min. The solvent was later outgassed in situ and evaporated by the action of primary vacuum down to the desired loading, as monitored by weight change.

As soon as the saturation vapor pressure of the liquid was stabilized, perfectly known H_2 doses measured in the reference volume were submitted to the cell. Care was taken that the pressure in the cell was stabilized before introduction of the next dose. After each dose, the pressure of the gas was reduced from that measured in the reference volume due to expansion and solubilization in the confined liquid. All the experiments were performed at room temperature (284–289 K) in the pressure range 101–202 kPa. Precautions were taken to avoid any contamination from adsorption on γ-alumina on the measured solubilities.[19] H_2 solubilities are given as the ratio of the H_2 dissolved in the solvent to that in the gas phase (i.e. $\ell_{H2} = C_{H2}/C_{g,H2} = C_{H2}RT/P_{H2}$). Using the present protocol, H_2 solubilities were accurate to within 15%. Further details dealing with the calculations can be found in Ref. 20.

Results

Table 2 summarizes the results obtained for H_2 solubility in ethanol in different liquid-solid environments. As can be seen, within the limits of the experimental error, our protocol reproduces fairly well published data in bulk ethanol (row 1).[23] Moreover, the solubility of H_2 dissolved in the solvent containing the porous solid (row 2) also approaches the bulk solubility value. On the opposite, H_2 solubility shows an increase up to four to five times over the bulk value when the solvent is confined in the solid mesopores (row 3), namely for solvent loadings lower than the total pore volume of the solid.

Figure 5 plots the concentration of dissolved hydrogen as a function of pressure in ethanol confined in γ-alumina for different nanoliquid sizes ranging from 4 to 9 nm. As can be seen, regardless of the liquid loading, H_2 concentration evolves linearly with pressure under confinement. Moreover, H_2 solubility increases with a reduction of the liquid loading in alumina, which implies in its turn a reduction of the pore size filled by the liquid or nanoliquid size. The solubility turns into bulk values when the whole solid is soaked by the liquid.

Figure 6 shows the effect of nanoliquid size on H_2 solubility in ethanol confined in γ-alumina. As can be seen, H_2 solubility is dramatically enhanced over the bulk value for nanoliquid sizes lower than 9 nm, as long as gas-liquid interfaces are confined in the mesoporous system. In contrast, bulk solubility values tend to be recovered for higher nanoliquid sizes, which corresponds to the situation where the solid is completely soaked by the liquid (row 2 in Table 2). The results shown in Figure 6 confirm the idea put forward in Ref. 19 that gas solubility is only enhanced as long as gas-liquid interfaces are located at the level of the solid mesopores (i.e. for solvent loadings $<100\%$).

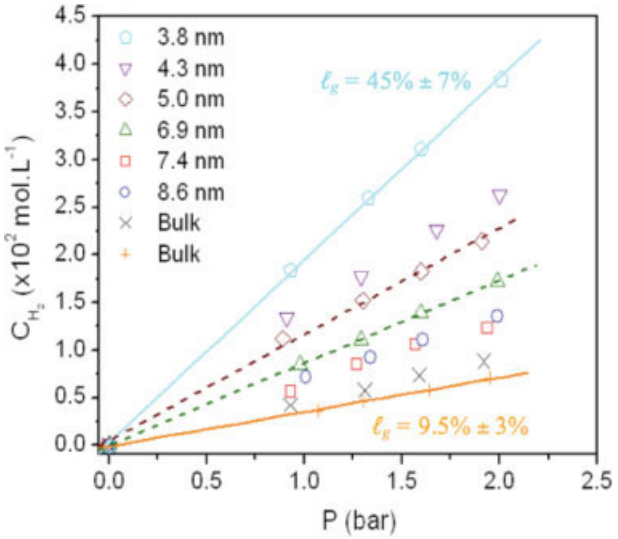

Figure 5. Evolution of the concentration of dissolved H_2 in ethanol as a function of pressure for different nanoliquid sizes.

[Color figure can be viewed in the online issue, which is available at www.interscience.wiley.com.]

Taking into account this experimental observation, gas solubility can be related to the nanoliquid size, $\bar{d}$, through a mass-balance based model as proposed previously.[19] Regarding a gas-liquid interface confined in a slit-like mesopore as illustrated in Figure 7 (for simplicity, the meniscus has been omitted and the pore depth has been equaled to the pore size), the overall H_2 solubility, ℓ_{H2}, can be obtained from a mass balance as follows

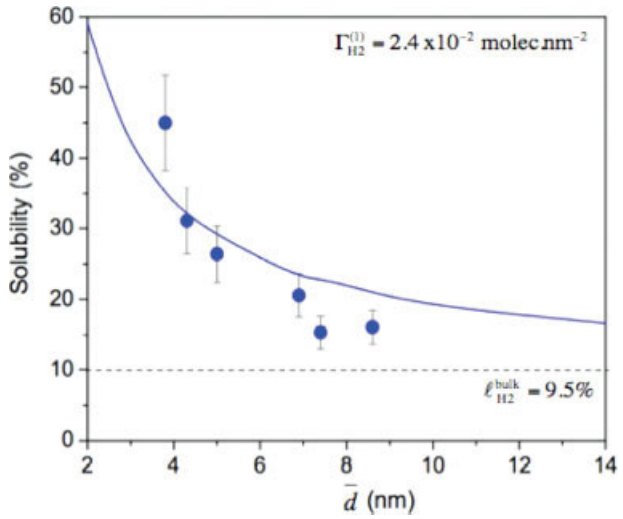

Figure 6. Pressure evolution of the concentration of dissolved H_2 in ethanol with pressure as a function of the nanoliquid size.

The solid and dashed lines correspond, respectively, to the fittings to Eq. 2 and to bulk solubility values. [Color figure can be viewed in the online issue, which is available at www.interscience.wiley.com.]

$$n_{H2} = n^{bulk}_{H2} + n^{int}_{H2}$$

$$C_L V^T = C^{bulk}_L V^{bulk} + C^{int}_L V^{int} \quad (V^T = V^{bulk} + V^{int})$$

$$\ell_g V^T = \ell^{bulk}_g V^{bulk} + \ell^{int}_g V^{int}$$

$$\ell_g = \ell^{bulk}_g + \frac{V^{int}}{V^T}\left(\ell^{int}_g - \ell^{bulk}_g\right)$$

where ℓ^{bulk}_{H2} and ℓ^{int}_{H2} are, respectively, the bulk and interfacial H_2 solubility. Assuming now that that the thickness of the gas-liquid interface, z, approaches the molecular size of H_2 (2.9 Å), $V^{int} / V^T \approx z/d$, the overall H_2 solubility, ℓ_{H2}, can be approached as follows for a mean pore size (i.e. nanoliquid size) $\bar{d}$ (Eq. 2)

$$\ell_{H2} \approx \ell^{bulk}_{H2} + \frac{z}{\bar{d}}\left(\ell^{int}_{H2} - \ell^{bulk}_{H2}\right) \tag{2}$$

The interfacial H_2 solubility can be related to the surface excess concentration of H_2 at the gas-liquid interface, $\Gamma^{(1)}_{H2}$, according to Eq. 3

$$\ell^{int}_{H2} = \frac{\Gamma^{(1)}_{H2}}{z C_{g,H2}} \tag{3}$$

Introducing Eq. 3 into Eq. 2, the following final expression is obtained for the overall gas solubility (Eq. 4)

$$\ell_{H2} = \ell^{bulk}_{H2} + \frac{1}{\bar{d}}\left(\frac{\Gamma^{(1)}_{H2}}{C_{g,H2}} + z\ell^{bulk}_{H2}\right) \tag{4}$$

Discussion: icCMRs vs. Nanoliquids

Increased gas solubility in nanoliquids

The experimental trends of H_2 solubility in ethanol with the nanoliquid size depicted in Figure 5 and summarized in Table 2 are qualitatively consistent with those found by ^{1}H-RMN in our previous study[19] for CH_4 and C_2H_6 in CCl_4 and CS_2. H_2 solubility is increased up to four to five times for

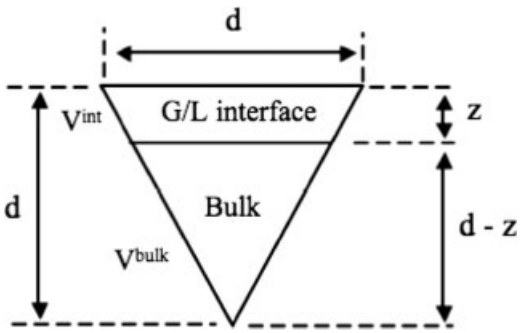

Figure 7. Simplified visualization of a liquid confined in a slit-like mesopore with a size and depth equaling to *d* and a confined gas-liquid interface with thickness *z*.

The meniscus has been omitted for simplicity. The volume of the confined liquid, V^T, can be expressed as $V^T = V^{bulk} + V^{int}$.

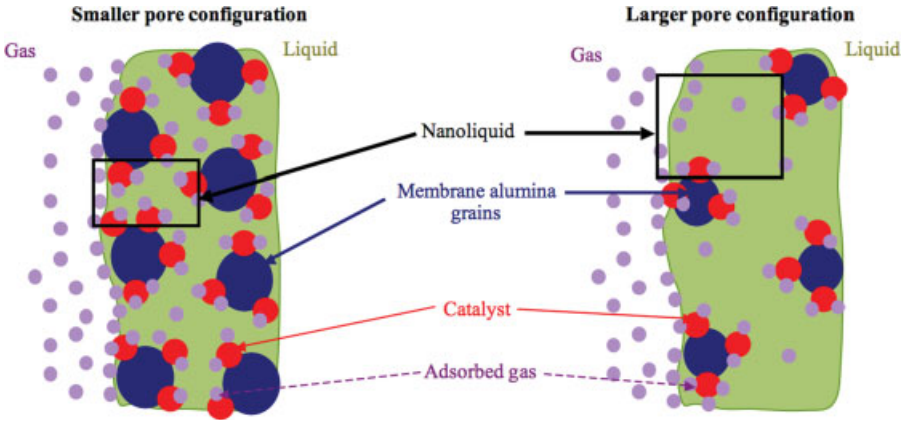

Figure 8. Scheme of a mesoporous layer showing the intimate gas-liquid-catalyst contact at the nanoscale in configuration 1 (gas in, liquid out) for (left) small-sized mesopores (<10 nm) and (right) larger-sized mesopores (>20 nm).

[Color figure can be viewed in the online issue, which is available at www.interscience.wiley.com.]

nanoliquid sizes lower than 5 nm while bulk solubility tends to be recovered beyond 15 nm.

Figure 6 shows that Eq. 2 predicts fairly well the experimental trend of H_2 solubility data with the nanoliquid size. The fitted surface excess concentration of H_2 in ethanol confined in γ-alumina is $\Gamma_{H2}^{(1)} = 2.4 \times 10^{-2}$ mol nm^{-2} at 101 kPa H_2 pressure and room temperature.

To evaluate the validity of this fitted parameter, an independent estimation was carried out. The variation of surface tension of the H_2/ethanol system with hydrostatic pressure has been estimated by the Macleod-Sugden correlation.[24] From this plot, the Gibbs equation leads to a value of surface excess concentration, $\Gamma_{H2}^{(1)} = 1.2 \times 10^{-2}$ mol nm^{-2}. Considering the totally independent approaches, both values are comparable. Moreover, the model predicts recovery of bulk solubility for nanoliquid sizes beyond 15–20 nm.

Formation of nanoliquids in icCMRs

To relate the increased solubility in nanoliquids to the enhanced catalysis of icCMRs, let us first discuss the formation of confined liquids in membrane porous layers according to the general configurations displayed in Figure 1.

In configuration 1 (gas in, liquid out, see Figure 1 on top), the gas is in direct contact with the catalyst nanoparticles surrounded by nanosized liquids. On the opposite, when operated using configuration 2 (gas out, liquid in, see Figure 1 on bottom), a direct contact between the gas and nanosized liquids surrounding the catalyst cannot be established, the gas-liquid interface being located within the support macropores. Therefore, on the basis of the influence of nanoliquid formation, configuration 1 appears more favorable to catalytic performance. Let us now examine in more detail the influence of the nanoliquid size on the catalytic performance of icCMRs when operated in this configuration.

Catalytic performance vs. nanoliquid size

First of all, the mesoporous layer is expected to be practically completely filled with the liquid at conventional transmembrane pressures due to capillary forces. Nevertheless, depending on the mean pore size of the catalytic top layer, the nanoliquid size is expected to be smaller for top layers made of smaller-sized mesopores (i.e. <10 nm) than for larger ones.

Figure 8 illustrates this nanoliquid size effect on the catalyst environment in a catalytic contactor operated in configuration 1. Qualitatively, the ratio of gas molecules, including those adsorbed on the gas-liquid interface, over the catalyst surface is larger in smaller pores when considering the same sample volume. Moreover, in smaller pores, the catalyst is, in average, closer to the gas-liquid interface.

Quantitatively, in configuration 1, the catalyst could benefit from the large amount of H_2 available in the nanoliquid when compared to a bulk situation in a conventional reactor. According to the plots in Figure 4, the surface excess concentration of H_2, ℓ_{H2}^{int}, is 2 orders of magnitude higher than the bulk solubility (9.5%). Let us consider $\ell_{H2}^{int} = \Gamma_{H2}^{(1)}/zC_{H2}$ (with $\Gamma_{H2}^{(1)} = 2.4 \times 10^{-2}$ mol nm^{-2}, $z = 0.2$ nm, and $C_{H2} = 0.04$ mol l^{-1}), leading to a value of $\ell_{H2}^{int} \approx 500\%$. This much higher local concentration of H_2 compared to the bulk might therefore contribute positively to the kinetics of the reaction of nitrobenzene hydrogenation.

On the basis of physically and chemically well-founded assumptions with respect to the reaction mechanism,[25–27] the kinetics of nitrobenzene hydrogenation catalyzed by noble metals is usually described through a Langmuir-Hinshelwood type model stemming from noncompetitive adsorption of nitrobenzene and hydrogen (Eq. 5)[28,29]

$$r = \frac{kK_{NB}K_{H2}C_{NB}C_{H2}}{(1 + K_{NB}C_{NB})(1 + K_{H2}C_{H2})} \quad (5)$$

The model Eq. 5 applies to a situation where, although most of the catalyst surface is covered by chemisorbed nitrobenzene, enough surface is still accessible to H_2 for adsorption. Furthermore, it is also assumed that an active site consists of two adjacent metal atoms onto which H_2 dissociates. For convenience, Eq. 5 can be rewritten in the form

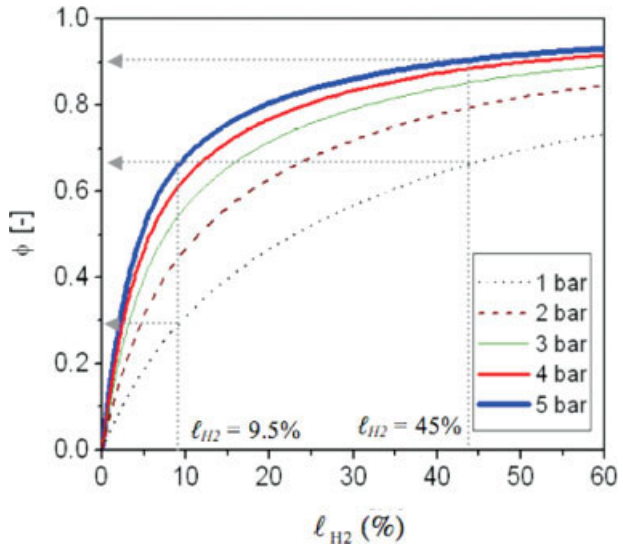

Figure 9. Evolution of function $\phi(C_{H2})$ at 323 K with H_2 solubility in ethanol at room temperature.

[Color figure can be viewed in the online issue, which is available at www.interscience.wiley.com.]

$$r = \frac{kK_{NB}C_{NB}}{(1 + K_{NB}C_{NB})}\phi(C_{H2}) \tag{6}$$

where

$$\phi(C_{H2}) = \frac{K_{H2}C_{H2}}{(1 + K_{H2}C_{H2})} \tag{7}$$

The function ϕ described by Eq. 7 can be rewritten by expressing the H_2 concentration in terms of ℓ_{H2}

$$\phi(\ell_{H2}) = \frac{K_{H2}(P_{H2}\ell_{H2}/RT)}{[1 + K_{H2}(P_{H2}\ell_{H2}/RT)]} \tag{8}$$

Assuming that the dissolved H_2 is at equilibrium with the gas phase, the increased catalytic activity in icCMRs using configuration 1 could be ascribed to an asymptotic increase of function ϕ toward 1. As an example, Figure 9 shows the evolution of function ϕ with the solubility of H_2 in ethanol at room temperature. The value of $K_{H2} = 134.1$ l mol^{-1} at 298 K, fitted from published H_2 adsorption data on Pt,[30] was used in these calculations.

As can be deduced from Figure 9, under conventional reactor conditions ($\ell_{H2} = 9.5\%$), it can be seen that a change from 1 to 3 bar has a large influence on ϕ because of the sharp increase of the plots at low abscissa values. On the contrary, for larger values of H_2 solubility due to nanoliquid formation (icCMR case operated in configuration 1), it can be seen that a change in pressure has a much more limited effect. This effect of H_2 pressure on the kinetics (value of ϕ) is in good keeping with the observed kinetic orders of H_2 in the different types of reactors (see Table 1). From a mathematical point of view, this increase of function ϕ approaching to saturation could simplify Eq. 4, eliminating the influence of H_2 concentration. This would translate into a zero-order dependence of the reaction rate on H_2 pressure.

In addition, the intimate contact between the gas, the nanoliquid and the catalyst makes the concentration in the vicinity of the latter practically constant during the reaction. This idea is sustained by the experimental observation that using ethanol pre-saturated with H_2 keeps the reaction almost rate unchanged.[12]

In contrast, when dealing with icCMRs operated in configuration 2, the apparent order for H_2 tends to 1 because function ϕ is far from the asymptote. In this configuration, the H_2 surface coverage of the catalyst is expected to be much lower, as the H_2 concentration in ethanol corresponds now to the bulk value. Accordingly, as reported in Ref. 12, additional supply of H_2 by pre-saturation of the solvent significantly promotes the reaction rate.

Finally, despite the increased H_2 adsorption on the catalyst using icCMRs in configuration 1, this reactor does not offer higher reaction rates when compared to those obtained in a slurry-type reactor (see Table 1). This is likely because of the fact that the direct comparison between both performances is made difficult owing to the very different reactor nature. However, it could be anticipated that in the case of an icCMR, the long diffusional path of nitrobenzene from the outer surface to the nanoliquid zone in the mesoporous layer might restrict the reaction rate. This has been demonstrated by Torres et al.[31] when modeling nitrobenzene hydrogenation in an icCMR and by Peureux[12] from the analysis of the apparent activation energy of the system. This limitation is evidenced from the experimental observation that the apparent order for nitrobenzene in an icCMR operated in configuration 1 lies in the range 0.3–0.6 (see Table 1) depending on the temperature (a higher order is obtained at higher temperatures due to the higher catalytic activity), while this order is 0 when the reaction is performed in a slurry-type reactor. This is why, as it has been addressed in recent publications,[9–11,32] it seems better to operate using an intermediate configuration where the liquid is kept mostly out of the porous membrane. In this system, the liquid located on the inner side and the gas pushes the gas-liquid interface deep within the porous system and as close as possible to the mesoporous catalytic layer. This might help reducing the diffusional path of the solute to the catalytic zone while maintaining the positive effect of nanoliquid formation described in this article.

Conclusions

Hydrogen solubility in ethanol increases dramatically over the corresponding bulk value (up to five times) when tuning the nanoliquid size to values in the range 4–15 nm. This *oversolubility* effect has been evidenced when considering a gas-liquid interface confined in solid mesopores. Although the bulk Henry's Law constant no longer applies in these conditions, gas solubility also increases linearly with pressure for these systems. On the opposite, when the liquid is confined but the gas-liquid interface is kept outside of the pores, the solubility is reduced to bulk values. This becomes true when the pore size exceeds 15 nm.

The increased gas solubility in mesoconfined solvents seems to be a key factor in explaining the enhanced catalytic activities found in interfacial contactors CMRs. These results reinforce the idea that the intimate contact between the gas and the catalyst surrounded by nanosized liquids (configuration 1) is the underlying phenomenon that explains the apparent H_2-zero-order kinetics for the nitrobenzene

hydrogenation reaction. These conclusions have stimulated novel configurations of interfacial contactors CMRs for other reactions of industrial interest.[9–11,32]

Acknowledgments

This work was supported by the French Agence Nationale de la Recherche (project Sursol/Nano JC05-43390) and the Marie Curie Program of the European Union (project Oversol/Nano). The authors express their gratitude to C. Daniel and E. Landrivon for the conception of the equipment and technical assistance, and Dr. V. Rakotovao for performing the H_2 solubility measurements in ethanol.

Notation

C = concentration (mol m^{-3})
d = pore size (nm)
$\overline{d}$ = nanoliquid mean size defined by Eq. 1 (nm)
ℓ_{H2} = H_2 solubility (%)
f = solvent loading
k = kinetic constant (mol s^{-1} cm^{-2}Pt)
K = adsorption constant (mol m^{-3})
P = pressure (Pa)
R = constant of gases (8.314 Pa m^3 mol^{-1} K^{-1})
$2t$ = statistical thickness of the pore wall (nm)
T = temperature (K)
V = volume (m^3)
z = gas-liquid interface thickness (nm)

Greek letters

$\Gamma^{(1)}$ = surface excess concentration (mol nm^{-2})
ϕ = function defined by Eq. 4

Subscripts

g = gas
H_2 = hydrogen
NB = nitrobenzene

Superscripts

bulk = bulk phase
Int = interface

Literature Cited

1. Cini P, Harold MP. Experimental study of the multiphase catalyst. *AIChE J*. 1991;37:997–1008.
2. Reif M, Dittmeyer R. Porous catalytically active ceramic membranes for gas-liquid reactions: a comparison between catalytic diffuser and forced through flow concept. *Catal Today*. 2003;82:3–14.
3. Dittmeyer R, Höllein V, Daub K. Membrane reactors for hydrogenation and dehydrogenation processes based on supported palladium. *J Mol Catal A*. 2001;173:135–184.
4. Peureux J, Torres M, Mozzanega H, Giroir-Fedler A, Dalmon J-A. Nitrobenzene liquid-phase hydrogenation in a membrane reactor. *Catal Today*. 1995;25:409–415.
5. Iojoiu EE, Walmsey JC, Raeder H, Bredesen R, Miachon S, Dalmon J-A. Comparison of different support types for the preparation of nanostructured catalytic membranes. *Rev Adv Mater Sci*. 2003;5:160–165.
6. Iojoiu EE, Miachon S, Dalmon J-A. Progress in performance and stability of a contactor-type catalytic membane contactor for wet air oxidation. *Top Catal*. 2005;33:135–139.
7. Uzio D, Miachon S, Dalmon J-A. Controlled Pt deposition in membrane mesoporous top layers. *Catal Today*. 2003;82:67–74.
8. Perez V, Miachon S, Dalmon J-A, Bredesen R, Pettersen G, Raeder H, Simon CH. Preparation and characterization of a Pt/ceramic catalytic membrane. *Sep Purif Technol*. 2001;25:33–38.
9. Vospernik M, Pintar A, Bercic G, Levec J. Mass transfer studies in gas-liquid-solid membrane contactors. *Catal Today*. 2003;79–80: 169–179.
10. Bercic G, Pintar A, Levec J. Positioning of the reaction zone for gas-liquid reactions in catalytic membrane reactor by coupling results of mass transport and chemical reaction study. *Catal Today*. 2005;105:589–597.
11. Vospernik M, Pintar A, Bercic G, Levec J, Walmsey JC, Raeder H, Iojoiu EE, Miachon S, Dalmon J-A. Performance of catalytic membrane reactor in multiphase reactions. *Chem Eng Sci*. 2004;59:5363–5372.
12. Peureux J. *Étude de Réacteurs Catalytiques à Membrane*, PhD Thesis. France: Université Claude Bernard-Lyon 1, 1994.
13. Torres M. *Étude et Modélisation d'un Membranaire Appliqué à des Reactions Triphasiques*, PhD Thesis. France: Université Claude Bernard-Lyon 1, 1993.
14. Iojoiu EE, Miachon S, Landrivon E, Walmsey JC, Raeder H, Dalmon J-A. The "Watercatox" process: wet air oxidation of industrial effluents in a catalytic membrane reactor. First report on contactor CMR up-scaling to pilot unit. *Catal Today*. 2006;118:246–252.
15. Miachon S, Perez V, Crehan G, Torp EG, Raeder H, Bredesen R, Dalmon J-A. Comparison of contactor catalytic membrane reactor with a conventional reactor: example of wet air oxidation. *Catal Today*. 2003;82:75–81.
16. Raeder H, Bredesen R, Crehan G, Miachon S, Dalmon J-A, Pintar A, Levec J, Torp EG. A wet air oxidation process using a catalytic membrane contactor. *Sep Purif Technol*. 2003;32:349–355.
17. Gelb LD, Gubbins KE, Radhakrishnan R, Sliwinska-Bartkowiak M. Phase separation in confined systems. *Rep Prog Phys*. 1999;62: 1573–1659.
18. Christenson HK. Confinement effects on freezing and melting. *J Phys Condens Matter*. 2001;13:R95–R133.
19. Miachon S, Syakaev VV, Rakhmatullin A, Pera-Titus M, Caldarelli S, Dalmon J-A. Higher gas solubility in nanoliquids? *Chemphyschem*. 2008;9:78–82.
20. El-Chahal R. *Sursolubilité de l'hydrogène à l'échelle Nanométrique*, Master Thesis. France: Université Claude Bernard-Lyon 1, 2007.
21. Morishige K, Shikimi M. Adsorption hysteresis and pore critical temperature in a single cylindrical pore. *J Chem Phys*. 1998;108: 7821–7824.
22. Tzevelekos KP, Kikkinides ES, Stubos AK, Kainourgiakis ME, Kanellopoulos NK. On the possibility of characterizing mesoporous materials by permeability measurements of condensable vapors: theory and experiments. *Adv Colloid Int Sci*. 1998;76–77:373–388.
23. Stephen H, Stephen T, editors. *Solubilities of Inorganic and Organic Compounds, Vol. I: Binary Systems*, part 1. Oxford, London: Pergamon Press, 1963.
24. Reid RC, Prausnitz JM, Poling BE. *The Properties of Gases and Liquids*, 4th ed. New York: McGraw-Hill, 1987.
25. Gelder EA, Jackson D, Lok CM. The hydrogenation of nitrobenzene to aniline: a new mechanism. *Chem Commun*. 2005;4:522–524.
26. Haber F. Gradual electrolytic reduction of nitrobenzene with limited cathode potential. *Z Elektrochem*. 1898;4:506–513.
27. Turek F, Geike R. Kinetics of the hydrogenation of nitrobenzene to aniline in liquid-phase. *Chem Tech*. 1981;33:24–28.
28. Turek F, Geike R, Lange R. Liquid-phase hydrogenation of nitrobenzene in a slurry reactor. *Chem Eng Process*. 1986;20:213–219.
29. Petrov L, Kumbilieva K, Kirkov N. Kinetic model of nitrobenzene hydrogenation to aniline over industrial copper catalyst considering the effects of mass transfer and deactivation. *Appl Catal*. 1990;59: 31–43.
30. Washburn EW, editor. *International Critical Tables of Numerical Data, Physics, Chemistry and Technology*, 1st electronic ed. New York: Knovel, 2003:1926–1930.
31. Torres M, Sanchez J, Dalmon J-A, Bernauer B, Lieto J. Modelling and simulation of a three-phase catalytic membrane reactor for nitrobenzene hydrogenation. *Ind Eng Chem Res*. 1994;33:2421–2425.
32. Iojoiu EE, Walmsey JC, Raeder H, Miachon S, Dalmon J-A. Catalytic membrane structure influence on the pressure effects in an interfacial contactor catalytic membrane reactor applied to wet air oxidation. *Catal Today*. 2005;104:329–335.

Manuscript received Apr. 16, 2008, and revision received July 28, 2008.